Journal of Materials Chemistry C

Accepted Manuscript

This article can be cited before page numbers have been issued, to do this please use: M. Melucci, M. Zambianchi, E. Benvenuti, C. bettini, C. Zanardi , R. Seeber, D. Gentili, M. Cavallini, M. Muccini, V. biondo, C. Soldano, G. Generali and S. Toffanin, *J. Mater. Chem. C*, 2016, DOI: 10.1039/C6TC02949C.

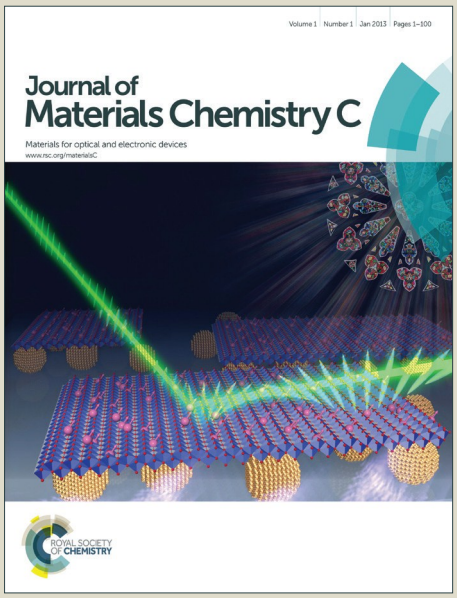

ROYAL SOCIETY OF CHEMISTRY

www.rsc.org/materialsC

DOI: 10.1039/C6TC02949C

Journal of Materials Chemistry C

ARTICLE

Anthracene-based molecular emitters for non-doped deep-blue organic light emitting transistors

Received 00th January 20xx,
Accepted 00th January 20xx

DOI: 10.1039/x0xx00000x

www.rsc.org/

M. Zambianchi,[a,†] E. Benvenuti, [b,†] C. Bettini, [a] C. Zanardi,[c] R. Seeber, [c] D. Gentili, [b] M. Cavallini, [b] M. Muccini, [b] V. Biondo, [d] C. Soldano, [d] G. Generali, [d] S. Toffanin, [b,*] and M. Melucci. [a,*]

A new anthracene-based twisted oligomer combining the rigid anthracene-xylene core to diphenylamine ends 4,4'-(anthracene-9,10-diyl)bis(2,5-dimethyl-*N*,*N*-diphenylaniline), **DiPAXA** is herein presented as efficient and deep blue emitter material. By exploiting **DiPAXA** as emissive layer and 2,7-dioctyl[1]benzothieno[3,2-b][1]benzothiophene (C8-BTBT) as p-type semiconducting layer, we realize a blue emitting unipolar light emitting transistor (OLET) with a maximum external quantum efficiency (EQE) of 0.13 %, charge mobility up to 0.32 cm^2/Vs and CIE color coordinates of (0.18, 0.21) , i.e. closer to currently available standards (PAL, NTSC). Moreover, comparison with other anthracene-based blue emitters highlights the suitability of the family of twisted anthracene-xylene compounds for unipolar blue OLETs applications as a result of the enhanced performances in terms of CIE coordinates and light emission output of newly synthesized **DiPAXA**.

1. Introduction

The development of efficient blue emitting organic materials has received a growing interest in the last decade for their potential applications as emissive layers in organic light emitting diodes devices (OLEDs) suitable for full color displays fabrication.[1-5] Different molecular structures including carbazole-dimesitylborane,[6] imidazole-p-triphenylamine derivatives, [7] among the others have been implemented so far and tested as blue emitters in both host-guest and single-component emission layer in OLEDs (i.e. metal-free complexes). It is highly preferable to implement single-component emission layer in multilayer organic optoelectronic devices. The constraints on the HOMO/LUMO level energetics in host-guest systems, which guarantee both efficient energy transfer and intense deep blue emission from the dopants, are, in fact, not easily satisfied in multilayer/multicomponent OLEDs. Furthermore, given the intrinsic high efficiency of the single-component emissive material, there are potentially more available recombination sites with respect to the host-guest system. Finally, the fabrication process of organic optoelectronic devices is simplified in the case of single-component emission layer.

The common motif of the proposed molecular structures in targeting blue emission requirement lies in the reduced π-conjugation extent that prevents red-shifted emission and strong crystallization tendency in films.

The single-material emission layer can be implemented in a multistack configuration also in organic light-emitting transistors (OLETs). [8-12] OLETs offer the possibility to combine in a single device the electrical switching capability of a transistor with the light-emission function, thereby reducing in principle the complexity of next-generation pixel circuitry.[13] However, it is rather difficult to find candidates for OLETs realization, from well-established OLED materials, since most of these do not exhibit high-performance field-effect characteristics, probably mostly due to their amorphous aggregation in solid state.

Given the limited number of efficient electroluminescent organic small molecules with good ambipolar mobility values, [14-17] a successfully strategy for improving OLET light emission performance consists in implementing a bilayer film comprising a charge-transport layer and a light-emitting layer as device active region. [18,19] Indeed, the bilayer configuration allows the decoupling of the region of high charge-carrier density from the light emission region so that the photo-physical processes such as lateral charge transport, exciton formation and radiative deactivation can be optimized independently. [20,22]

In single-layer OLET device configuration, Adachi *et al.* introduced the use of a bis(stryryl)biphenyl derivative as blue-emitting ambipolar organic semiconductor. [23] The same group

[a] *Consiglio Nazionale delle Ricerche, Istituto per la Sintesi Organica e la Fotoreattività, (CNR-ISOF), via P. Gobetti 101, 40129 Bologna, Italy *Email - mmelucci@isof.cnr.it*
[b] *Consiglio Nazionale delle Ricerche, Istituto per lo Studio dei Materiali Nanostrutturati (CNR-ISMN), via P. Gobetti 101, 40129 Bologna, Italy*
[c] *Department of Chemical and Geological Sciences University of Modena and Reggio Emilia via G. Campi 103 - 41125 Modena (Italy)*
[d] *E.T.C. srl, Via P. Gobetti 101, 40129 Bologna, Italy*
† These authors contributed equally.

Electronic Supplementary Information (ESI) available: Differential Scanning Calorimetry, Optical properties of BDNA and BD3 materials in solution and thin films, Morphology of BDNA, BD3 and DiPAXA, OLET performance for BDNA and BD3. See DOI: 10.1039/x0xx00000x

View Article Online
DOI: 10.1039/C6TC02949C

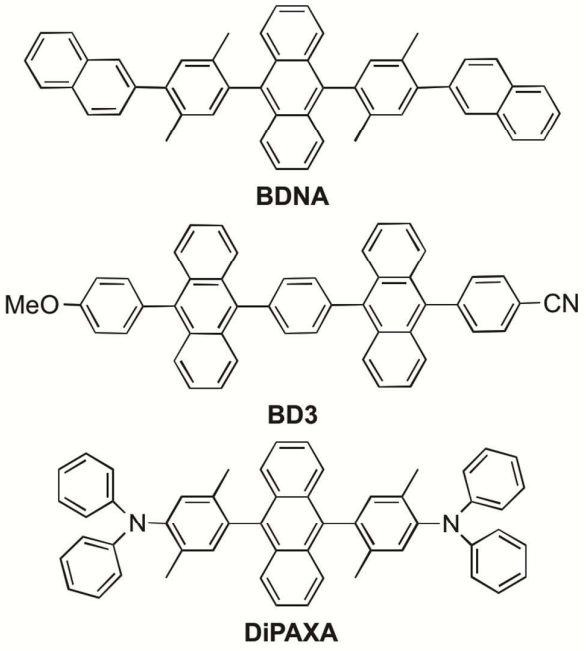

Chart 1. Molecular structure of the anthracene derivatives, BDNA[25] and BD3 [27] and of DiPAXA studied herein.

reported a blue-emitting OLET with external quantum efficiency (EQE) up to 0.2% by implementing a fluorene asymmetric derivative in a single-layer bottom-contact/bottom-gate (BC/BG) OLET by exploiting two-colors electrode configuration. [24] However, using a single material for transporting hole carriers and emitting light leads to poor device performance in terms of hole mobility and source-drain current (around 10^{-6} cm^2/Vs and 2 μA, respectively). Moreover, the emitted light intensity was observed to increase with the gate voltage up to a maximum and to decrease by further increase of the gate voltage and corresponding current.

This evidence was correlated to the use of single-layer device in a bottom-contact/bottom-gate configuration.

In this work, we use a bilayer active region OLET in top-contact/bottom-gate (TC/BG) configuration as a device platform for comparing and screening three blue emitters based on anthracene derivatives (Chart 1) as possible class of materials for OLETs fabrication. A new anthracene derivative, namely DiPAXA, is synthetized according to the structure-design requirements that are typically used for defining new molecule classes for efficient blue-emitting OLEDs. [25-27]

Indeed, anthracene-based materials have emerged as valuable materials for blue OLEDs realization. In particular, the anthracene core substituted at the 9,10-positions are related to excellent photoluminescence and electroluminescence properties, poorly crystalline film morphology and HOMO-LUMO energy levels fine-tunability.[28-33] Kim *et al.* demonstrated by means of a rationally designed class of anthracene-based emitters that anthracene substitution with bulky substituents provide steric hindrance, which prevents intermolecular interactions and reduces self-quenching effects leading to improved EL performances. [25,26]

Recently, the effect of the substitution of anthracene with 2,5-dimethyl-xylene on the optical and morphology properties of the resulting molecular derivatives has been investigated. For the twisted BDNA derivative (chart 1) OLEDs CIE coordinates of (0.159; 0.072) and maximum external quantum efficiency (EQE) of 5.26% were reported.[25] The effect of molecular symmetry on the color coordinates and device efficiency was also investigated. Bisanthracene-based donor acceptor type derivatives with symmetric or asymmetric structure, have been also developed with the aim of further rigidifying the system to prevent π-conjugation. For the asymmetric BD3 derivative (chart 1) EQE of 4.2% with CIE color coordinates of (0.15; 0.06) were measured which are close to the CIE of the high definition standard blue. [27]

On this basis, here we consider two anthracene derivatives which have already demonstrated suitable for OLEDs application and are characterized by a twisted and rigid symmetric conformation, namely BDNA[25] and the bisanthracene BD3[27] (chart 1), as well as a newly designed compound, DiPAXA. The structural motif of DiPAXA includes the twisted anthracene core and a diphenylamine end moieties that are commonly related to high solid state emission efficiency in OLED addressed organic matrixes. The anthracene-based materials in chart 1 were used as emissive layers in bilayer device architecture with a high mobility p-type field-effect semiconductor layer, namely 2,7-dioctyl[1]benzothieno[3,2-b][1]benzothiophene (C8-BTBT).[34,35]

2. Experimental

2.1 Synthesis

General: 9,10-bis(4-bromo-2,5-dimethylphenyl)-anthracene and 9,10-bis(2,5-dimethyl-4-(naphthalen-2-yl)phenyl)-anthracene (BDNA) were prepared as previously described. [25] BD3 was prepared according to ref. 26.

Synthesis of 9,10-bis(2,5-dimethyl-4-(N,N-diphenylaniline-2-yl)phenyl)anthracene, DiPAXA, ***3***: 9,10-Bis(4-bromo-2,5-dimethylphenyl)anthracene, **1** (600 mg, 1.10 mmol), diphenylamine, **2** (410 mg, 2.43 mmol) and sodium tert-butoxide (265 mg, 2.76 mmol), were mixed in dry toluene (30 mL), then bis(tri-tert-butylphosphine)palladium(0) $Pd(t\text{-}Bu_3P)_2$ (56 mg, 0.11 mmol) was added at 60 °C.

The solution was refluxed for 24 h, then the solvent was removed under vacuum, and the crude product was washed in hexane. The residue was purified by flash chromatography (silica gel column and hexane-CH_2Cl_2 solvent gradients). The fractions containing the product were combined, the solvent evaporated, and the residue washed in pentane gave a white solid (556 mg, 70% yield).

M.p. > 280 °C; DE-MS (m/z): 720 (M^{+}); absorption maximum, 397 nm, emission maximum, 493 nm in DCM; ^{1}H NMR (400 MHz, $CDCl_3$), δ [ppm]: 7.68-7.66 (m, 4 H), 7.43-7.40 (m, 4H), 7.33-7.30 (m, 8H), 7.23 (bs, 4H), 7.17-7.15 (m, 8H), 7.01-6.98 (m, 4H), 2.08 (s, 6H), 1.83 (s, 6H). ^{13}C NMR (400 MHz, $CDCl_3$), δ

View Article Online
DOI: 10.1039/C6TC02949C

[ppm]: 147.6, 144.7, 137.1, 137.0, 136.2, 136.0, 135.9, 134.5, 134.4, 133.7, 130.8, 129.8, 129.1, 126.8, 125.2, 121.6, 121.4, 19.4, 19.3, 18.2, 18.1. Anal. Calcd for $C_{54}H_{44}N_2$ (720.94): C, 89.96; H, 6.15. Found: C, 89.90; H, 6.21.

2.2 Theoretical calculations

The geometry of all the compounds has been optimized in their ground state in vacuum using the B3LYP[36, 37] change-correlation functional and 6-311+G* basis set as implemented in the Gamess code.[38] TDDFT calculations of the lowest singlet-singlet excitation $S_0 \rightarrow S_1$ have been performed to compute the optical gap E_g.

2.3 Thin film preparation

Thin films of organic material were deposited on quartz by thermal evaporation in a home-made high-vacuum deposition chamber at room temperature at a base pressure of 10^{-6} mbar. The material was deposited at a rate of 1Å/s.

2.4 Optical characterization

Thin-film UV-visible absorption spectra were recorded with a JASCO V-550 spectrophotometer. Steady-state photo-luminescence (PL) was excited using a CW He–Cd laser at a wavelength of 325 nm and collected under transmission conditions (no color filter was necessary for truncating laser excitation).

PL emission was collected with a calibrated optical multi-channel analyzer (PMA-11, Hamamatsu). Quantum yield measurements of thin-films were carried out by a stand-alone and automatic absolute PL Quantum Yield (PLQY) measurements System (C9920-02, Hamamatsu). The measurements were performed in ambient conditions and exciting the PL emission at the thin-film absorption maximum wavelength.

2.5 Electrochemical characterization

Cyclic Voltammetry (CV) was performed with an Autolab PGSTAT12 (Ecochemie). A 2 mm Pt disc was used as the working electrode. It was cleaned with 0.3 and 0.05 µm Al_2O_3 powder and rinsed with water in an ultrasonic bath before use. The electrochemical cell was completed with Pt and Ag wires as counter and pseudo-reference electrodes, respectively. The potentials were referred to the ferricinium/ferrocene (Fc^+/Fc) redox couple by adding a small crystal of Fc into the electrochemical cell. CV traces have been collected either in a 1 mM DiPAXA or BDNA CH_2Cl_2 or THF solutions, also containing 0.1 $(n\text{-}Bu)_4NPF_6$ as supporting electrolyte.

2.6 Device fabrication

Organic light emitting transistors were fabricated on glass/ITO substrates where ITO works as gate electrode and PMMA (450nm) is used as gate dielectric. The organic active region consists of a stacked bi-layer formed from a high-mobility *p*-type semiconductor C8-BTBT [34, 35] (45 nm) in direct contact with the dielectric layer and a compact thin film made of DiPAXA (60 nm) (see Figure 3a). The thickness of 45 nm for C8-BTBT was chosen as a good compromise between thickness and values of charge mobility. A charge mobility value of about 3 cm^2/Vs was measured for single-layer C8BTBT device with thickness of 45 nm.

The organic bilayer stack and the on-top metal electrodes were deposited by thermal evaporation by means of shadow masks in a home-made high-vacuum deposition chamber at room temperature at a base pressure of 10^{-6} mbar. 70 nm thick silver source and drain electrodes are then evaporated. Devices have the following characteristics: 12 mm channel width, 70 µm channel length, 500 µm wide source and drain electrodes. The electrical and optical measurements were performed in an inert atmosphere drybox. The light output was measured through the bottom of the substrate (*i.e.* through the gate electrode) with a silicon photodiode (sensitivity of 0.38A W^{-1} at 600 nm) placed in contact with the devices to enable collection of all emitted photons.

3. Results and discussion

3.1 Synthesis

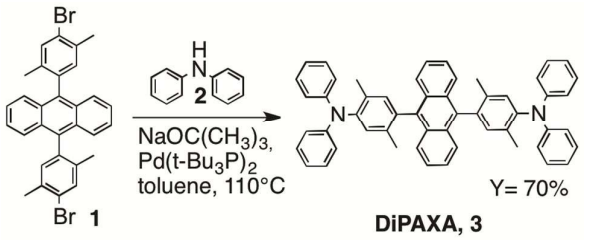

Scheme 1. Synthetic route to DiPAXA.

DiPAXA was synthesized starting from 9,10-Bis(4-bromo-2,5-dimethylphenyl)anthracene, **1** and diphenylamine **2** under Pd catalysis in the presence of NaOtBu as depicted in scheme 1. Compound **1** was prepared by nucleophilic addition reaction of antraquinone and monolithiated dibromoxylane according to already described procedure.[25]

Differential Scanning Calorimetry, DSC (Figure S1, ESI) under nitrogen atmosphere, reveals a melting transition at about 370°C suggesting a high thermal stability.

3.2 Optoelectronic properties

The optoelectronic properties of the newly synthesized DiPAXA were characterized by a combined theoretical and experimental approach and compared to those of the already known anthracene-based compounds BD3 and BDNA. Theoretical calculations by using density function theory (DFT) B3LYP/6-311+G* method were performed to calculate HOMO LUMO energy levels values and frontier orbital energy distribution. Results are shown in Figure 1. The calculated molecular geometry for DiPAXA shows an almost orthogonal arrangement between the anthracene and the xylene moiety. Calculations also show that while the HOMO electron density is mainly localized on the xylene-diphenylamine arm, the LUMO density is mainly located on the anthracene core. The non-planar overall configuration limits the degree of conjugation, which positively affects both the emission feature

View Article Online
DOI: 10.1039/C6TC02949C

and the crystallization capability. An optical gap $S_0 \rightarrow S_1$ of 2.90 eV (427 nm) is computed for the molecule in vacuum. Interestingly, calculations additionally compute an almost degenerate conformer (ΔE = 3 meV) with the xylene moieties specular to each other. However, both the relaxed geometry

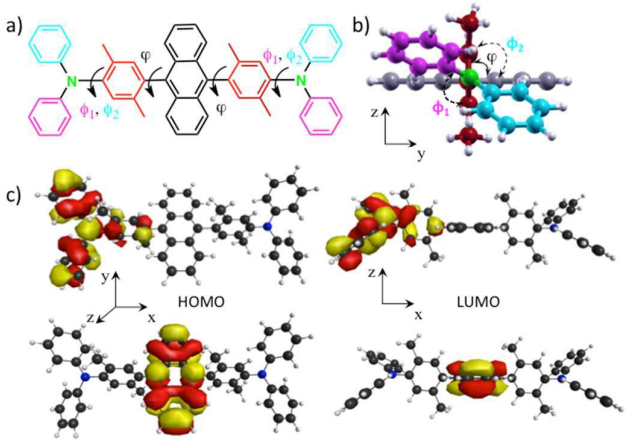

Figure 1. a) molecular sketch and b) optimized geometry of DiPAXA with torsional angles ϕ between anthracene and xylene and φ between xylene and diphenylamine ϕ_1= 117°, ϕ_2=126°, φ [illegible]c) DiPAXA frontier molecular orbitals (HOMO left column, LUMO right column).

(i.e. the torsional angles) and the electronic structure (i.e. HOMO, LUMO and E_g) are consistent one with the other. The optical properties of DiPAXA in dilute solution and vacuum sublimed film are reported in Figure 2a. The absorption spectra in both solution and film show the typical vibrational pattern of the anthracene moiety with peaks located at about 340, 350, 380 and 400 nm. The photoluminescence (PL) spectra are broad and unstructured with maximum-emission peaks in the blue range that are located at 469 and 457 nm for solution and thin-film respectively. A blue-shift in the main emission peak of about 10 nm is observed in the thin-film PL spectrum. The optical features of the emission profiles highlight not only that the molecule preserves the non-planar configuration in thin-film, but also that the overall molecular π-conjugation is further reduced possibly due to increase in steric hindrance as the moieties arrange in solid state. Differently, BDNA presents structured PL spectra both in solution and in thin film (Figure S2, ESI). In particular, the thin-film PL spectrum presents at least three clear peaks with large full-width-at-the-half-maximum value (around 90 nm). Even though there is almost no Stoke shift in both solution and thin-film in the case of BDNA, the emission profile features in solid state are possibly detrimental in achieving suitable CIE coordinates in the final device (see after). Interestingly, the DiPAXA and BDNA present similar values of PL quantum yield in both solution and films, namely around 82-86% to 50% respectively. As a final remark, we observed that the introduction of less-bulky but asymmetric end-substituents in the anthracene core (as in the case of BD3) results in a PL spectrum profile (Figure S3, ESI) similar to DiPAXA, which is expected to be well-suited for blue-emitting optoelectronic device. However, the BD3 PL quantum yield value in solid state is very low with respect to the other two compounds (around 7%). From spectroscopic investigation, we can assess that the molecule-design strategy for DiPAXA is effective in achieving deep-blue emitting compounds with high quantum yield in solid state.

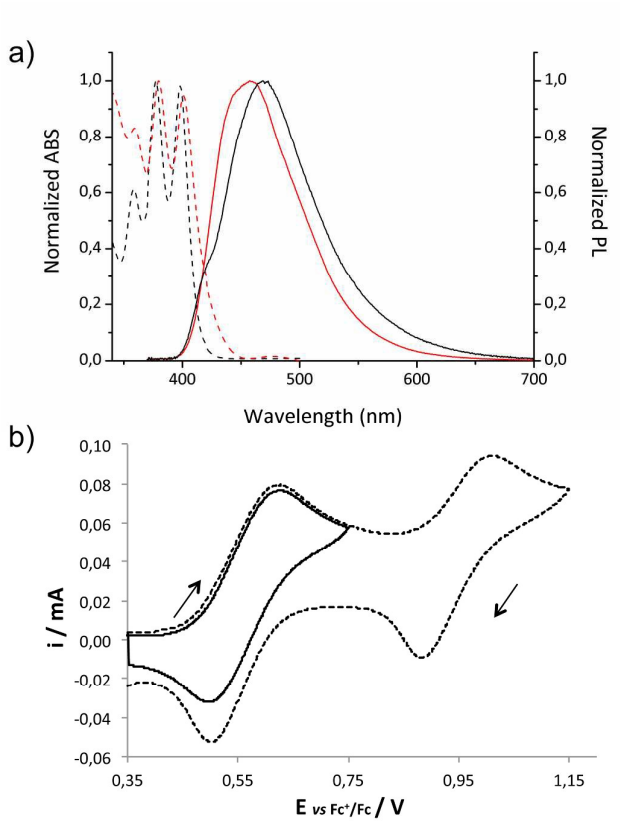

Figure 2. Absorption (dotted lines) and emission (solid lines) spectra of DiPAXA a) in CH_2Cl_2 solution (10^{-5}M) (black lines) and b) in neat films (thickness 50 nm, red lines). Spectra of BDNA and BD3 are reported in the ESI. b) CV traces of 1 mM DiPAXA in CH_2Cl_2/nBu_4NPF_6 solution; 1 Vs^{-1} potential scan rate (a positive feedback for IR compensation was applied).

Table 1. Optoelectronic data.

item	BD3	BDNA	DiPAXA
λ_{abs}[a] (nm)	359,378, 399	342,358, 378,398	358, 377, 398
λ_{abs}[b] (nm)	364,384, 405	344,360, 379,401	359, 380, 401
λ_{em}[a] (nm)	430, (443)	411, 430, 453, 485	469, (418)
λ_{em}[b] (nm)	(448), 480	411, 434, 466, 501	457 (455)
PLQY[c] (%)	20/7	82/50	86/50
HOMO (eV) (theo/exp)	-5.34/ -6.01[d]	-5.25/ -5.91[e]	-5,17/- 5.71[e]
LUMO (eV) (theo/exp)	-2.40/- 3.03[d]	-2.15/ -2.88[f]	-2.26/ -2.71[f]
E_g (eV)	2.98[d]	3.04[g]	3.00

a) CH_2Cl_2 solutions, b) film (50nm), c) solution/film, d) from ref. 26, e) E_{HOMO} = e(4.68+E°_{ox}), where E°_{ox} was computed vs. SCE, f) calculated from the optical band gap. E_g is the optical energy gap, g) from ref. 25.

View Article Online
DOI: 10.1039/C6TC02949C

CV experiments were carried out in order to calculate the value of HOMO and LUMO energy levels. A value of -5.71 eV was calculated from experiments carried out both in CH_2Cl_2 and THF solutions, revealing that this compound is reversibly oxidized with $E_{1/2}$=+0,56 V vs Fe^+/Fe (see Figure 2b). This value,

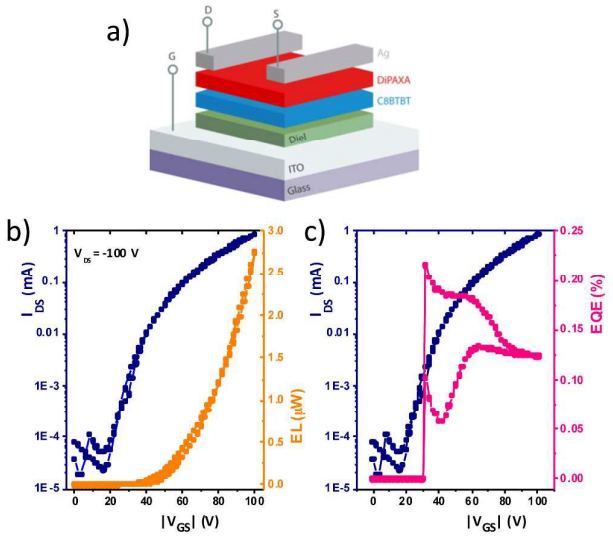

Figure 3. (a) Schematic representation of the organic light emitting transistors in bi-layer configuration. The dielectric layer is PMMA and the organic active region is formed by a p-type semiconductor layer (C8-BTBT, 45nm) in direct contact with the dielectric and a DiPAXA thin layer (60 nm). (b-c) Saturation transfer curves (@ V_{DS} = -100V) with corresponding (b) emitted optical power and (c) external quantum efficiency (EQE) of the device.

lower with respect to both BD3 and BDNA is consistent with the electron-donating mesomeric effect induced by the nitrogen atom conjugated to the anthracene moiety. Unfortunately, any attempts to compute LUMO energy level from CV traces failed.

Actually deposition of a film is also observed by polarizing the working electrode at potential values higher than those required for the first oxidation process, i.e. suitable to achieve oxidation of phenyl moieties.

3.4 Characterization of unipolar bilayer OLET devices

The device configuration consists of a bilayer of DIPAXA and 2,7-dioctyl[1]benzothieno[3,2-b][1]benzothiophene C8BTBT)[34, 35] p-type semiconductor deposited onto PMMA/ITO/glass substrate (details in the experimental section and sketch of the device in Figure 3a). Figure 3b shows the energy diagram of the entire device. Saturation transfer curves (V_{DS} = -100V) are shown in Figure 3 as well as the measured emitted optical power and calculated EQE.

As expected, the device behaves only as a *p*-type transistor, with C8BTBT dominating the field-effect transport within the device. The transistor is clearly in its *OFF*-state for biases below |25V| and light is completely absent. The onset of light is found experimentally at around |40V|, likely due to the energy barrier for electrons injection at silver/DiPAXA interface, and the maximum output optical power of about 2.75 μW is reached at the maximum I_{DS} current of about 1mA. The transistor shows a value of the I_{ON}/I_{OFF} ratio of approximately 10^4-10^5.

Figure 3c shows the external quantum efficiency, which correlates the number of available charge carriers with the number of emitted photons upon radiative recombination; we

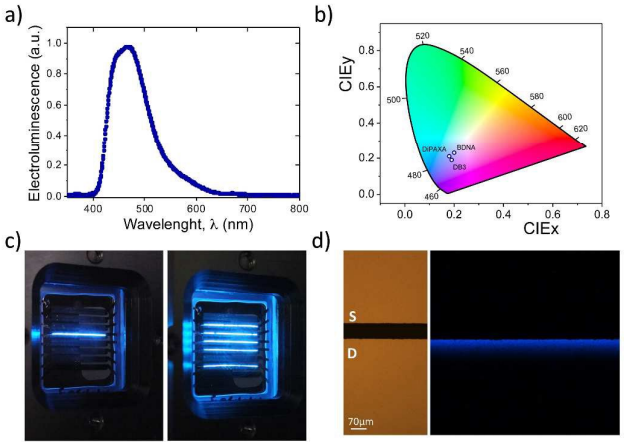

Figure 4. a) Normalized electroluminescence (EL) spectra of one of our representative DiPAXA-OLETs with (b) XY color map plane (CIE standard) indicating the color coordinates of various emitting materials analyzed in this work (DiPAXA (0.18; 0.21). CIE map has been adapted from an online available source file from OriginLab®. Color coordinates of BDNA and DB3 corresponding devices are also reported for reference. (c) Optical images of one of our DiPAXA organic light emitting transistors where one or multiple individual linear devices are in their ON-state. (d) Microscope image on one of our representative DiPAXA OLETs in (left) OFF- and (right) ON state, showing the localization of the light emission below the drain electrode.

found that in the limit V_{DS}= V_{GS}= -100 V the value of EQE is approximately 0.125 %, about one order of magnitude larger than the corresponding values obtained for the other anthracene-based materials in the same device configuration (see Figure S5, ESI and Table 2 below). Despite the different device architecture and materials used, this value of efficiency resides within the same range for other bilayer OLET devices [20-22].

Figure 4a shows the normalized electroluminescence (EL) spectra of one of representative DiPAXA-OLETs biased at V_{DS}=V_{GS}=-100V which shows a broad peak (FWHM = 90nm) centred at around 470 nm.

From the device EL spectrum, we were also able to determine the color coordinates of our organic light emitting transistors (Figure 4b), which are x = 0.18 and y = 0.21. The coordinates of the DB3 and BDNA are also reported for comparison (see Table 2). It can be seen that the emission of the DiPAXA based device is characterized by a deeper blue component, thus leading to a blue emission closer to currently available standards (PAL, NTSC) as it was expected from the optical spectroscopic investigation.[39]

View Article Online
DOI: 10.1039/C6TC02949C

Table 2. Summary of electrical and optical properties of organic light emitting transistors fabricated with various emitting materials discussed in this work.

item	$\|I_{DS}$-max$\|$ (μA)	μ_p (cm^2/Vs)	$\|V_{th}$, p$\|$ (V)	EL max (μW)	EQE@ 100V (%)	CIE coord. (X,Y)
BD3	329	0.15	41.7	0.16	0.019	(0.19, 0.19)
BDNA	880	0.46	34	0.76	0.034	(0.2, 0.23)
DiPAXA	860	0.32	25.8	2.75	0.125	(0.18, 0.21)

Prior to optical characterization carried out in atmosphere, as-fabricated devices were encapsulated inside the glovebox using a glass coverslip and an ultraviolet-cured epoxy sealant. A getter (Dryflex, provided by SAES-GETTERS) was also used to prevent any deterioration of the sample. Figure 4c shows optical images of DiPAXA OLETs while mounted on a sample holder in their ON-state for one or multiple devices. The microscope image showing in more details the channel area of an individual device is shown in fig. 4d. It can be seen that when the OLET is lit, the light emission is located below the drain electrode.[40]

Despite a similar PLQY value and almost comparable mobility values (see Tables 1 and 2), the EQE measured for DiPAXA device was one order of magnitude higher than that of BDNA based device. However, AFM analysis (Figure S4, ESI) revealed that BDNA presented morphological features more favorable to charge injection and transport (i.e. lower rms roughness and higher film homogeneity and compactness). Indeed, a possible explanation for the different behavior can rely on the materials/electrodes energy level match. The energy level diagrams (Figure 5), shows that DiPAXA has a better energy alignment with C8BTBT in comparison with BDNA, given that the DiPAXA HOMO level is higher than the C8BTBT one (about 0.2 eV). This clearly indicates that thanks to this energetic mismatch, in DiPAXA-based device holes are accumulated at the emitters/C8BTBT interface (emitter side). Conversely, In the case of BDNA (and even worse in the case of BD3) there is no energetic mismatch (and for BD3 the mismatch is even inverted) and holes are likely to be preferentially accumulated at the p-type semiconductor. Regarding electrons, in all the device structures the LUMO energy barrier hinders the charge percolation into C8BTBT layer. Thus, the electrons are localized within BDNA and DiPAXA. By virtue of the previous considerations, excitons can be formed efficiently only in DiPAXA-based devices, given the coexistence of charges of opposite signs in the emissive layer. This possible light-formation mechanism is corroborated by the one-order-of-magnitude higher optical power measured in DiPAXA-based OLETs with respect to BDNA and DB3. Further dedicated investigations will be carried out to fully elucidate this preferred injection mechanism and to further enhance the device efficiencies. In this respect, the use of different materials for the drain electrodes (*i.e.* low work-function metals such as calcium) or of a passivation layer on top of the emitting layer will be taken into account.[22]

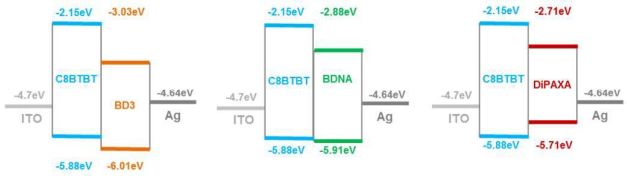

Figure 5. Schematic representation of the experimental energy level diagrams of the OLET device for BD3, BDNA and DiPAXA materials.

Conclusions

In conclusions, we have demonstrated the suitability of twisted anthracene molecular emitters as a class of blue emitting materials for OLET realization. A new material namely DiPAXA was synthetized and characterized in bilayer-configuration device. The performance of DiPAXA was compared to that of two other anthracene-based materials namely BDNA and BD3 already used for OLEDs applications. DiPAXA showed slightly deeper blue electroluminescence and higher external quantum efficiency with respect to BDNA and BD3. However, all the compounds demonstrated light emission correlated to field-effect charge transport conditions. Further work will be focused on the tailoring of the degree of twist of bulky substituents at the 9,10-positions anthracene derivatives by chemical design in order to guarantee effective increase in light formation and emission in solid state. Moreover, introduction of the anthracene-based single-component emissive layer in a trilayer OLET architecture [8] where both hole and electron currents are maximized and balanced, is currently under investigation.

Acknowledgements

MM thanks Dr. Federico Gallino (SAES Getters) for the helpful discussion. CS would like to acknowledge financial support from FIRB project RBAP115AYN “Metal oxide nanostructures: multifunctionalities and applications”.

Notes and references

1 M.A. McCarthy, B. Liu, E.P. Donoghue, I. Kravchenko, D.Y. Kim, F. So and A.G. Rinzler, *Science*, 2011, **332**, 570.
2 E. J. Feldmeier, M. Schidleja, C. Melzer and Heinz von Seggern, *Adv. Mater.*, 2010, **20**, 1.
3 S-J. Su, C. Cai and J. Kido, *Chem. Mater.,* 2011, **23**, 274.
4 Y. Fukuda, T. Watanabe, T. Wakimoto, S. Miyaguchi and M. Tsuchida, *Synt. Metals*, 2000, **111–112,** 1.
5 H. Sirringhaus, *Adv. Mater.*, 2014, **26**, 1319.
6 S. L. Lin, L.H. Chan, R.H. Lee, M.Y. Yen, W. J. Kuo, C. T. Chen and R. J. Jeng, *Adv. Mater.* 2008, **20**, 3947.
7 Y. Zhang, S.-L. Lai, Q.-X.Tong, M.-F. Lo, T.-WaiNg, M.-Y. Chan, Z.-C. Wen, J. He, K.-S. Jeff, X.-L. Tang, W.-M. Liu, C.-C. Ko, P.-F. Wang and C.-S. Lee, *Chem. Mater.* 2012, **24**, 61.
8 M. Muccini, *Nature Materials* 2006, **5**, 605.

View Article Online
DOI: 10.1039/C6TC02949C

9 R. Capelli, S. Toffanin, G. Generali, H. Usta, A. Facchetti and M. Muccini, *Nature Materials* 2010, **9**, 496.
10 M. Muccini and S. Toffanin, Organic Light-Emitting Transistors: Towards the Next Generation Display Technology, Ed. Wiley-Science Wise Co-Publication, 2016.
11 M. Muccini, W. Koopman and S. Toffanin, *Laser Photonics Rev.* 2012, **6**, 258.
12 S. Toffanin, S. Kim, S. Cavallini, M. Natali, V. Benfenati J. J. Amsden, David L. Kaplan, R. Zamboni, M. Muccini and F. G. Omenetto, *Applied Physics Letters* 2012, **101**, 091110.
13 H-H. Hsieh, W-C. Chen, G. Generali, C. Soldano, R. D'Alpaos, G. Turatti, V. Biondo, M. Muccini, E. Huitema and A. Facchetti, *Proc. of Society of Information Display (SID),* 2016, **54-3**.
14 M. Durso, C. Bettini, A. Zanelli, M. Gazzano, M. G. Lobello, F. De Angelis, V. Biondo, D. Gentili, R. Capelli, M. Cavallini, S. Toffanin, M. Muccini and M. Melucci, *Org. Electron*., 2013, **14**, 3089.
15 M. Melucci, M. Zambianchi, L. Favaretto, M. Gazzano, A. Zanelli, M. Monari, R. Capelli, S. Troisi, S. Toffanin and M. Muccini, *Chem. Commun*., 2011, **47**, 11840.
16 M. Melucci, L. Favaretto, M. Zambianchi, M. Durso, M. Gazzano, A. Zanelli, M. Monari, M. G. Lobello, F. De Angelis, V. Biondo, G. Generali, S. Troisi, W. Koopman, S. Toffanin, R. Capelli and M. Muccini, *Chem. Mater*., 2013, **25**, 668.
17 M. Melucci, M. Durso, C. Bettini, M. Gazzano, L. Maini, S. Toffanin, S. Cavallini, M. Cavallini, D. Gentili, V. Biondo, G. Generali, F. Gallino, R. Capelli and M. Muccini, *J. Mater. Chem. C*, 2014, **2**, 3448.
18 R. Capelli, F. Dinelli, S. Toffanin, F. Todescato, M. Murgia, M. Muccini, A. Facchetti and T. J. Marks *J. Phys. Chem*. C 2008, **112**, 1299312999.
19 R. Capelli, F. Dinelli, M.A. Loi, M. Murgia, R. Zamboni and M. Muccini, *Journal of Physics: Condensed Matter* 18 (33), S2127.
20 E. B. Namdas, P. Ledochowitsch, J. D. Yuen, D. Moses and A.J. Heeger *Appl. Phys. Lett.* 2008, **92**, 183304
21 B.B.Y. Hsu, J. Seifter, C.J.Takacs, C. Zhong, H-R. Tseng, I.D. Samuel, E. B. Namdas, G. C. Bazan, F. Bazan, Y. Cao and A. J. Heeger *ACS Nano* 2013, **7**, 2344.
22 J. H. Seo, E. B. Namdas, A. Gutacker, A. J. Heeger and G. C. Bazan. *Adv. Funct. Mater.* 2011, **21**,3667.
23 T. Sakanoue, M. Yahiro, C. Adachi, H. Uchiuzou, T. Takahashi and A. Toshimitsu, *Appl. Phys. Lett.* 2007, **90**, 171118.
24 T.-H. Ke, R. Gehlhaar, C.-H. Chen, J.-T Lin, C.-C. Wu and C. Adachi *Appl. Phys. Lett.* 2009, **94**, 153307.
25 H. Park, J. Lee, I. Kang, H. Y. Chu, J.-I. Lee, S.-K. Kwon and Y.-H. Kim, *J. Mater. Chem*., 2012, **22**, 2695.
26 Ran Kim, S. Lee, K.-H. Kim, Y.-J. Lee, S.-K. Kwon, J.-J. Kimand and Y.-H. Kim *Chem. Commun.,* 2013, **49**, 4664.
27 J.-Y. Hu, Y.-J. Pu, F. Satoh, S. Kawata, H. Katagiri, H. Sasabe and J. Kido *Adv. Funct. Mater.* 2014, **24**, 2064.
28 Y. H. Kim, H. C. Jeong, S. H. Kim, K. Y. Yang and S. K. Kwon, *Adv. Funct. Mater*., 2005, **15**, 1799.
29 Y. H. Kim, S. J. Lee, K. N. Byeon, J. S. Kim, S. C. Shin and S. K. Kwon, *Bull. Korean Chem. Soc.*, 2007, **28**, 443.
30 A. K. Kim, B. Yang, Y. Ma, J. H. Lee and J. W. Park, *J. Mater. Chem*., 2008, **18**, 3376.
31 M. K. Shin, S.O. Kim, H.T. Park, S.J. Park, H.S. Yu, Y.H. Kim and S. K. Kwon, *Dyes Pigm*., 2012, **92**, 1075.
32 J. K. Park, K. H. Lee, S. Kang, J. Y. Lee, J. S. Park, J. H. Seo, Y. K. Kimand, S. S. Yoon, *Org. Electron*., 2010, **11**, 905.
33 S.-H. Lin, F.-I. Wu, H.-Y. Tsai, P.-Y. Chou, H.-H. Chou, C.-H. Cheng and R.-S. Liu, *J. Mater. Chem.*, 2011, **21**, 8122.
34 T. Matsushima, A. S. D. Sandanayaka, Y. Esaki and C, Adachi *Scientific Reports* 2015, **5**:14547.
35 Y. Yuan, G. Giri, A, L. Ayzner, A. P. Zoombelt, S. C. B. Mannsfeld, J. Chen, D, Nordlund, M, F. Toney, J. Huang and Z. Bao, *Nat. Commun.* 2016, **5**:3005 and ref. therein.
36 A. D. Becke, *J. Chem. Phys*., 1993, **98**, 5648.
37 C. Lee, W. Yang and R. G. Parr, *Phys. Rev. B: Condens. Matter Mater. Phys*., 1988, **37**, 785.
38 M. W. Schmidt, K. K. Baldridge, J. A. Boatz, S. T. Elbert, M. S. Gordon, J. H. Jensen, S. Koseki, N. Matsunaga, K. A. Nguyen, S. Su, T. L. Windus, M. Dupuis and J. A. Montgomery, *J. Comput. Chem*., 1993, **14**, 1347.
39 T. C. Tsai, W.Y., L.-C. Chi, P.-T. Chou, *Organic Electronics,* 2009*,* **10**, 158.
40 S. Toffanin, R. Capelli, W. Koopman, G. Generali, S. Cavallini, A. Stefani, D. Saguatti, G. Ruani and M. Muccini, *Laser Photonics Rev.* 2013, **7**, 1011.

View Article Online
DOI: 10.1039/C6TC02949C

Table of Contents

Twisted anthracene derivatives including the newly synthesized DIPAXA compound, are here investigated as blue emitters in non doped organic light emitting transistors (OLETs). DIPAXA based device shows superior performance with maximum EQE of 0.13 %, charge mobility up to 0.32 cm^2/Vs and CIE color coordinates of (0.18, 0.21), highlighting the suitability of this class of materials for blue OLETs application.